

# DETECTION OF LANDSLIDES DUE TO THE 2013 THYPOON WIPHA FROM HIGH-RESOLUTION AIRBORNE SAR IMAGES

Wen Liu, Fumio Yamazaki

Graduated School of Engineering, Chiba University, Japan

## ABSTRACT

A strong typhoon hit the Pacific coast of Japan from the night of October 15th to the morning of 16th, 2013, and caused huge damages, especially in Izu-Oshima island, Tokyo. Synthetic aperture radar (SAR), which can observe the earth surface despite of weather conditions, is an effective tool to grasp damage situation caused by typhoons. In this study, pre-event Pi-SAR-L and post-event Pi-SAR-L2 airborne radar images with full polarizations were used to detect landslides and debris flows in Izu-Oshima. First, the extraction of potential landslide areas was carried out using only the post-event image by land-cover classification and from the standardized difference polarization index (NDPI). Then the difference of backscattering intensity between the pre- and post-event SAR images was calculated to extract potential landslides. In addition, a 5-m resolution digital elevation model (DEM) was introduced to remove errors. Finally, the results were verified through the comparison with the result from visual interpretation.

**Index Terms**— Izu-Oshima, Pi-SAR-L/L2, normalized difference polarization index (NDPI), full polarization

## 1. INTRODUCTION

Typhoon Wipha (also called the Typhoon No. 26, 2013 in Japan) originated from a tropical depression on October 8, 2013 and grew up to a typhoon on October 12. It affected the Pacific coast of Japan from the night of October 15th to the morning of 16th, 2013, and then weakened as an extratropical low-pressure system. The maximum wind speed reached 35 m/s with over 950 hPa atmospheric pressure. The moving track and its intensity change from October 9th to 18th are shown in Fig. 1(a) [1]. Due to its high wind speed and the large gale wind area, it caused huge damages in Japan, especially in Izu-Oshima island, Tokyo. One hundred (100) mm rainfall was recorded within one hour on the island, and the total rainfall in 24-hour was more than 800 mm. According to the report of the Fire and Disaster Management Agency, Japan, 39 people were killed or missing, 71 houses were completely collapsed and 25 buildings were severe damaged due to landslides and debris flows caused by this typhoon.

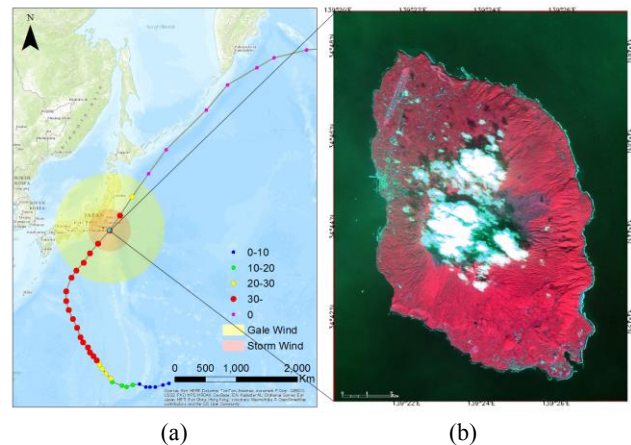


Fig. 1 Moving track and maximum wind-speed change of the 2013 Typhoon Wipha (a); a false-color composite image taken by FORMOSAT-2 satellite on Oct. 18, 2013 (b).

Remote sensing is an effective tool for emergency response after a natural disaster strikes. Although optical images could provide more detailed information, most of them were affected by cloud cover, especially in case of typhoon attack. A false-color composite image taken by FORMOSAT-2 satellite on October 18, 2013 (2 days after the typhoon passed by) is shown in Fig. 1(b), with 2-m spatial resolution. It is difficult to grasp damage situation from this optical image because thick clouds cover the central part of the island. Since Synthetic aperture radar (SAR) can observe the earth surface despite of weather condition, it is useful for detecting damages caused by typhoons [2]. In this study, the pre-event Pi-SAR-L and post-event Pi-SAR-L2 airborne radar data captured are used to extract landslides and debris flows in Izu-Oshima island, Japan. Potential landslide areas are detected based on the characteristics of different polarizations. A 5-m resolution digital elevation model (DEM) is introduced to remove the changes caused by the extension of urban areas. Finally, the extracted results are verified through the comparison with visual interpretation results.

## 2. IMAGE DATA AND PRE-PROCESSING

The pre- and post-event aerial SAR data over Izu-Oshima island, which is one of the most severely affected areas by the typhoon, are used in this study. The pre-event data was

Table 1. Comparison of the performances between the Pi-SAR-L and Pi-SAR-L2 sensors (cited from [3]).

Sensors	Pi-SAR-L	Pi-SAR-L2
Band width	50 MHz	85 MHz
Sampling frequency	61.275 MHz	100 MHz
Image width	≤ 15 km	≤ 20 km
Slant range resolution	2.5 m	1.76 m
Azimuth resolution (4 looks)	3.2 m	3.2 m
Incident angle	10–60 degree	10–62 degree
Polarimetry	full	full

taken on August 20, 2000 by Pi-SAR-L sensor, whereas the post-event data was taken on October 22, 2013 (one week after the typhoon hit) by Pi-SAR-L2 sensor. Pi-SAR was an airborne SAR system developed for earth measurement and disaster monitoring [3]. It carries two different frequencies antennas, L- and X-bands. Pi-SAR-L sensor was operated by Japan Aerospace Exploration Agency (JAXA) from 1996 to 2011, and its successor, Pi-SAR-L2 sensor, with higher resolution started observation from 2012. The performances of Pi-SAR-L and Pi-SAR-L2 sensors are shown in Table 1. Both the pre- and post-event SAR data were taken by the full polarimetry in a descending path. Although the spatial resolution of the post-event image was higher than the pre-event one, they were provided as the geo-coded intensity images in 2.5 m/pixel.

Due to the instability of aircraft, the pre- and post-event SAR data are not match even after geo-coding. Co-registration was carried out by setting 8 ground control points (GCPs) manually. Then the digital numbers (DNs) of the two images were transformed to the sigma naught value ( $\sigma^0$ ) according to the calibration parameters [3] by Eq. (1).

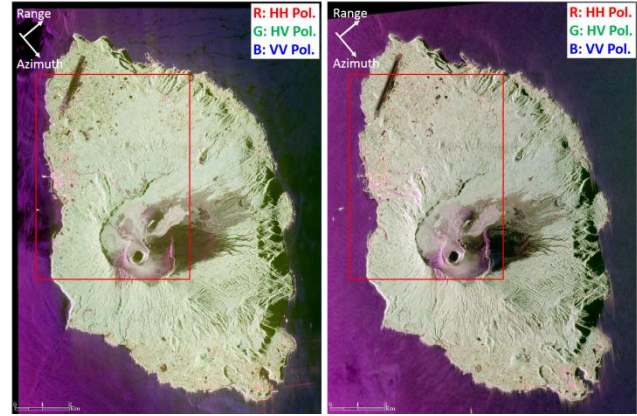
$$\sigma_{dB}^0 = 10 \cdot \log_{10} \langle DN^2 \rangle + CF \quad (1)$$

where  $CF$  is -74.11 dB for the Pi-SAR-L image and -79.88 dB for the Pi-SAR-L2 image;  $\langle \rangle$  represents a smoothing operation with a  $3 \times 3$  pixels window.

The pre-processed color composites using three polarizations are shown in Fig. 2. According to the color composites, most of the island was covered by vegetation excepting towns and lava desert in the east side of the Miharayama volcano. A large-scale debris flow that occurred in the west side of the volcano could be identified from color change after the typhoon. Since the time lag between the pre- and post-event images was more than 10 years, several urban land-use changes could be observed.

### 3. DETECTION OF LANDSLIDES AND DEBRIS FLOWS USING THE POST-EVENT SAR DATA

Since the pre-event archive data is unavailable in most cases of disasters, the extraction of landslides is carried out using only the post-event data first. Comparing with the single



(a) Aug. 30, 2000 (b) Oct. 22, 2013  
Fig. 2 Color composites of the pre-event Pi-SAR-L data taken on August 30, 2000 (a) and the post-event Pi-SAR-L2 data taken on October 22, 2013 covering the target area, Izu-Oshima island.

polarimetry SAR data, the full polarimetry (HH+HV+VH+VV) data can provide more surface information. Thus, the ISODATA unsupervised classification [4] was applied on the post-event Pi-SAR-L2 data to extract landslide affected areas. The post-event image with the four polarizations was classified into 8 classes automatically. Comparing with the color-composite image, 6 classes were assigned and shown in Fig. 3(a). The landslide areas show high backscattering intensity in the HH and VV polarizations, similar as built-up areas. Therefore, it was difficult to distinguish landslides (bare soil), built-up areas, and the edge of the crater from the classification result.

According to the recent study [5], the co- and cross-V polarization (VV and VH) are useful for the identification of geologic structure. Cao et al. [6] proposed the normalized difference polarization index (NDPI) to extract the geologic hazard using ENVISAT C-band data.

The NDPI was adopted in this study to detect landslide or debris flow areas from the post-event SAR image. Since the SAR data have been transformed into the backscattering coefficient after the radiometric calibration, which was in the range from -40.2 dB to 16.4 dB in the four polarizations, the equation for the NDPI was written as Eq. (2).

$$NDPI = \frac{(\sigma_{vv} + 50) - (\sigma_{vh} + 50)}{\sigma_{vv} + \sigma_{vh} + 100} \quad (2)$$

where  $\sigma_{vv}$  and  $\sigma_{vh}$  are the backscattering coefficients in the VV and VH polarizations, respectively.

Then the NDPI value between -1.0 and 1.0 was calculated and shown in Fig. 3(b). Since the HV and VH polarizations, which represent the volume scattering, show higher values in vegetated areas than other land covers. The vegetated areas show low NDPI values close to 0. Built-up areas with rougher surface than soils and rocks also show low NDPI values. The largest debris flow occurred in the west side of the volcano covered by trees before the typhoon attack, could be identified easily from Fig. 3(b) by high

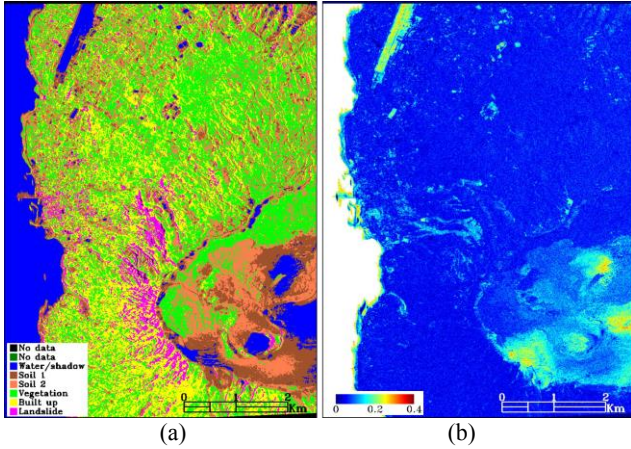


Fig. 3 The result of unsupervised classification with 8 classes for the full polarization post-event SAR data (a); the NDPI image obtained using the VH and VV polarizations after applying a water mask (b).

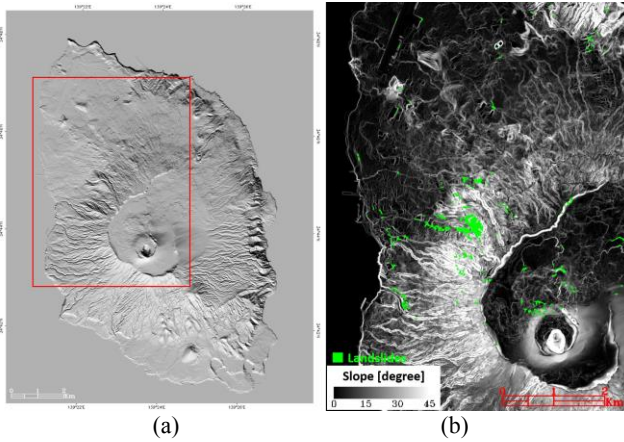


Fig. 4 Hill-shaded image made from a 5-m resolution digital elevation model provided by GSI [7] (a); the detected landslides using the NDPI value and the gradient of elevation (b).

NDPI values. Thus, a threshold value of the NDPI was set to extract debris flow and/or landslide affected areas.

Since the NDPI values for the geologic hazard areas are not the highest, the threshold value was set as the average value of the whole target area, which is 0.1 in this case. The areas with larger NDPI values than 0.1 were extracted. The sea, the soil areas around the crater and the airport runway with the smoothest surface show the highest NDPI values, and they were extracted as errors. But they could be distinguished using the classification result shown in Fig. 3(a) with the lowest backscattering intensity. Then the potential geologic hazard areas were obtained by removing the third class (blue one) from the extracted high NDPI areas. However, several built-up areas with the similar roughness as geologic hazard areas still exist in the detected result.

A 5-m resolution digital elevation model (DEM) built by the Geospatial Information Authority (GSI) of Japan [7] was introduced to improve the detected result. A hill-shaded

image of the DEM is shown in Fig. 4(a). The DEM data were re-sampled as 2.5 m/pixels to match with the Pi-SAR data. Then a slope map was calculated within a  $3 \times 3$  pixels window and is shown in Fig. 4(b) in a gray-scale. Since debris flows and landslides usually occur in sloping surfaces, the potential areas with the slope-angle higher than 10 degree were considered as the final results.

A clean-up process was applied to reduce small noises. The extract areas were grouped into objects. Then the objects smaller than 100 pixels (about 600 m<sup>2</sup>) were considered as noises, such as urban changes, and were removed from the results. The landslide areas detected using the unsupervised classification, the NDPI values and the gradient are shown in Fig. 4(b). A total area of 34.8 km<sup>2</sup> was detected as the areas affected by geologic hazards. It could be confirmed that two largest debris flows were detected successfully.

#### 4. DETECTION OF LANDSLIDES AND DEBRIS FLOWS USING THE TWO-TEMPORAL SAR DATA

Difference is the most popular operation for the change detection from multi-temporal images. However, the time lag between the pre- and post-event SAR data is large, more than 10 years. In addition, the pre- and post-event data were taken by the different sensors. The backscattering intensities of unchanged areas showed different values between the pre- and post-event images, even after the radiometric calibration. Thus it was difficult to detect the changes by comparing the two temporal intensity data directly. "Standardization" was carried out by subtracting the differences of two polarizations taken at the two times. Since most of the target areas were covered by vegetation before the typhoon, the HV polarization was used for extracting geological disasters that cause loss of vegetation. In this stage, the HH polarization was employed as the reference. Then the surface changes due to the typhoon were represented by the standardized difference ( $D_S$ ) as Eq. (3).

$$D_S = \langle \sigma_{hh}^0 - \sigma_{hv}^0 \rangle_{post} - \langle \sigma_{hh}^0 - \sigma_{hv}^0 \rangle_{pre} \quad (3)$$

where  $\sigma_{hh}^0$  and  $\sigma_{hv}^0$  are the backscatter coefficient (dB) in the HH and HV polarization, respectively;  $\langle \rangle$  represents a smoothing operation with a  $3 \times 3$  pixels window.

The obtained standardized difference is shown in Fig. 5(a) in rainbow color. After the standardization, the influence of the acquisition conditions was reduced. A high  $D_S$  value shows the decrease of the HV polarization due to landslides and debris flows. The areas with higher values than 2.5 dB, which is the sum of the average value and the standard deviation, were extracted as potential landslides/debris flows. However, the decreases of vegetation caused by urban development around the town also show high  $D_S$  values. Thus, the gradient of topography (slope angle) was introduced to remove these errors. The detected results after

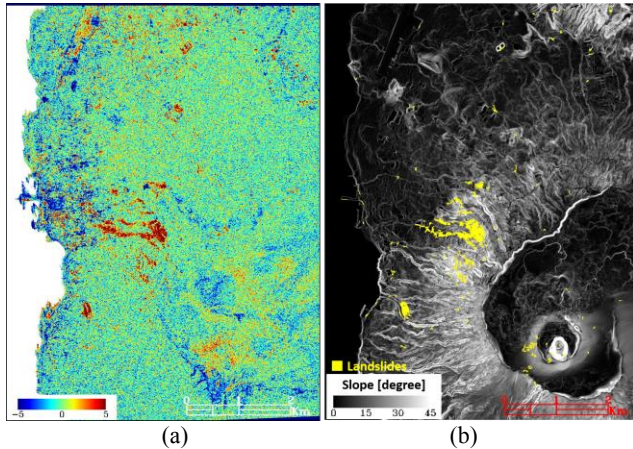


Fig. 5 Standardized difference between the pre- and post-event Pi-SAR data using the HH and HV polarizations (a); the detected landslides using the normalized difference and the gradient of elevation (b).

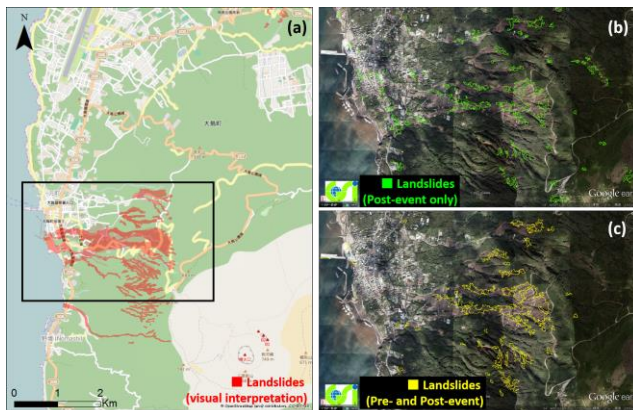


Fig. 6 Comparison of the visual interpretation [7] (a), the detected results using only the post-event image (b), the detected results using the pre- and post-event images (c). (b) and (c) are overlapping on a post-event aerial photograph taken by GSI on Oct. 17, 2013, which was used for visual interpretation.

cleaning-up small noises are shown in Fig. 5(b). A total area of 40.0 km<sup>2</sup> was detected as landslides or debris flows.

Comparing the result shown in Fig. 4(b) and Fig. 5(b), the errors due to unchanged built-up and soil areas could be avoided by adding the pre-event data. In contrast, the landslides occurred in soil or built-up areas before the typhoon could not be detected. The result of visual interpretation was introduced to verify our results, as shown in Fig. 6(a). A total area of 104.8 km<sup>2</sup> was extracted as landslides using aerial photographs taken by GSI on October 17 and 22, 2013. A close-up comparison is shown in Fig. 6(b) and (c). The detection using both the pre- and post-event data could extract the shape of landslides/debris flows more completely with less commission (false positive) errors. However, the extraction using only the past-event data also could give a reasonable overview of landslides.

## 5. CONCLUSIONS

The detection of landslides and debris flows occurred in Izu-Oshima island, Japan due to the 2013 Typhoon Wipha was carried out using Pi-SAR-L/L2 airborne full polarimetry data. The NDPI calculated from the VV and VH polarizations was used to extract potential landslide areas from only the post-event data. The standardized difference between the pre- and post-event HH and HV polarizations was obtained to detect landslides as well. In addition, the gradient from a 5-m resolution DEM was introduced to improve the detected results. Comparing with a visual interpretation result, the largest debris flows were detected successfully from the both methods. The detection using the two temporal SAR data show higher accuracy, but one using only the post-event data could also obtain a valid result.

## 10. ACKNOWLEDEMENT

Pi-SAR-L and Pi-SAR-L2 data used in this study are owned by Japan Aerospace Exploration Agency (JAXA), and the FORMOSAT-2 image is owned by the National Space Organization (NSPO) of Taiwan. The all imagery data were provided through the JAXA's working group on satellite image analysis in large-scale disasters.

## 11. REFERENCES

- [1] National Institute of Informatics (NII): <http://agora.ex.nii.ac.jp/digital-typhoon/summary/wnp/g/201326.html> en
- [2] W. Liu, M. Matsuoka, B. Adriano, E. Mas, and S. Koshimura, "Damage detection due to the Typhoon Haiyan from high-resolution SAR images," *2014 IEEE International Geoscience and Remote Sensing Symposium*, pp. 4828-4831, 2014.
- [3] Pi-SAR: <http://www.eorc.jaxa.jp/ALOS/Pi-SAR-L2>
- [4] Tou, J. T., and R. C. Gonzalez, *Pattern Recognition Principles*, Addison-Wesley Publishing Company, Massachusetts, 1974.
- [5] Q. Tan, S. Yang, and J. Hu, "Potentiality of radar remote sensing technology to geologic hazards," *Railway Investigation and Surveying*, 5, pp. 5-11, 2004.
- [6] Y. Cao, L. Yan, and Z. Zheng, "Extraction of information on geology hazard from multi-polarization SAR images," *The International Achieves of the Photogrammetry, Remote Sensing and Spatial Information Science*, XXXVII, pp. 1529-1532, 2008.
- [7] Geospatial Information Authority of Japan: <http://www.gsi.go.jp/kiban/index.html>